American Mineralogist, Volume 84, pages 1939–1949, 1999

Novel TEM approaches to imaging of microstructures in carbonates: Clues to growth mechanisms in calcite and dolomite

JEANNE PAQUETTE,[1,*] HOJATOLLAH VALI,[2] AND ERIC MOUNTJOY[1]

[1]Department of Earth and Planetary Sciences, McGill University, 3450 University Street, Montreal, Quebec H3A 2A7, Canada
[2]Electron Microscopy Centre, McGill University, 3640 University St., Montreal, Quebec H3A 2B2, Canada

ABSTRACT

Relating microstructures imaged by transmission electron microscopy (TEM) to specific growth mechanisms requires imaging of both the surface microtopography on crystal faces and its corresponding microstructure in the bulk crystal. Pt-C replicas of as-grown surfaces are ideally suited to this task, as they provide a high-resolution, nearly three-dimensional image of surface topography that can be correlated with microstructures visible in sections at high angle to the as-grown surface. Ultramicrotomy enables the preparation of ultrathin sections more quickly than conventional ion-thinning and can be used to investigate chemical heterogeneities by analytical electron microscopy (AEM). We evaluate the potential of both techniques for the study of microstructures in calcite and dolomite. (1) TEM images were obtained from Pt-C replicas of synthetic calcite. The as-grown $(10\bar{1}4)$ face of a Mg/Mn-doped crystal growth showed growth hillocks aligned along preferred orientations. In Pb/Mn/Sr-doped calcite, sections at high angle to as-grown faces showed a uniform microstructure in $\{10\bar{1}4\}$ sectors. The $\{01\bar{1}2\}$ sectors contained concentric zones that alternated from striated to uniform microstructures, suggesting periodic variations in growth rate and possibly in the growth mechanism. An oscillatory-zoned Mn-doped calcite showed fine-scale banding (30–150 mm) and periodic roughening of $(10\bar{1}4)$ surfaces that suggest repetitive transitions between growth mechanisms. (2) In sedimentary dolomites, Pt-C replicas of surfaces cleaved parallel to a $(10\bar{1}4)$ face showed a hillocky topography or smooth $(10\bar{1}4)$ surfaces modified by non-equivalent facets. Surfaces produced by cleavage at high angle to a $(10\bar{1}4)$ face exposed sectors with fine-scale banding crosscut by sharp boundaries, suggestive of closely spaced growth hillocks intercalated with non-equivalent subsectors. Ultrathin sections prepared by microtomy showed some disruption of the crystal structure but, in some dolomite samples, domains with distinctive microstructures similar in scale and shape to those seen in the Pt-C replica were identified. (3) The growth microstructures in $\{10\bar{1}4\}$ sectors of dolomite present striking similarities to the larger scale compositional zoning patterns produced by growth spirals in calcite doped with trace elements. At this stage, Pt-C replicas and ultramicrotomy can distinguish among dolomites that are petrographically very similar.

INTRODUCTION

Sedimentary carbonates, and specifically calcite and dolomite, commonly show important deviations in morphology, structure, stoichiometry, and/or cation ordering from their ideal crystalline structure (Goldsmith and Graf 1958; Reeder 1983). These imperfections are accommodated by various structural defects as documented by transmission electron microscopy (TEM) particularly of dolomite cf. review by Reeder (1992a). The orientation of microstructures such as modulation structure, Ca-rich ribbons, fine-scale banding within the growth sectors suggests that they are a product of the crystal growth mechanism. Relating these features to specific factors (e.g., degree of supersaturation, presence of growth inhibitors, Mg/Ca ratio of parent fluid) could help constrain the paleoenvironmental conditions that prevailed during the precipitation and diagenesis of sedimentary carbonates.

Relating microstructures to specific environmental parameters requires pristine, as-grown crystal faces, formed under known conditions be examined, so that their surface microtopography can be related to the distribution of microstructures preserved in the bulk crystal. Hence, synthetic calcite offers an ideal starting point. The orientation of steps and their relative rates of spreading are sensitive to the presence of foreign ions, the saturation state and the proportions of Ca^{2+} and CO_3^{2-} ions present in the parent solution (Paquette and Reeder 1995). These relationships can be described quantitatively from experiments where the surface topography is investigated in situ by atomic force microscopy (AFM) during the precipitation of calcite from an aqueous solution (e.g., Teng et al. 1998**)**. However, the thin overgrowths produced in a typical AFM experiment are not amenable to study by conventional TEM. Therefore we do not know yet if the height and

*E-mail: jeannep@geosci.lan.mcgill.ca

0003-004X/99/1112–1939$05.00

shape of growth islands or hillocks and the bunching of layers or the formation of facets on a crystal face produce characteristic microstructures once they are buried in the bulk crystal. AFM experiments are also generally restricted to freshly cleaved ($10\bar{1}4$) surfaces, imposed by the need for a flat substrate that is easy to orient for imaging. Therefore little is known of the growth mechanisms on other crystallographic surfaces and their potential for generating microstructures in the bulk crystal. However, a relationship between surface microtopography and compositional zoning patterns is well established, but only for hillocks and facets developed on a larger scale than features typically imaged by AFM. On faces where arrays of parallel growth steps cover areas severals tens or hundreds of micrometers across, compositional zoning patterns documented by electron probe microanalysis (EPMA) or cathodoluminescence (CL) microscopy can be related systematically to the orientation of steps that prevailed during growth from solution (Paquette and Reeder 1995). Elucidating the relationship of microstructures to near-atomic scale surface topography would be a significant step toward the interpretation of intracrystalline compositional heterogeneities found at the nanoscale.

Conventional TEM imaging of ion-thinned calcite foils has shown heterogeneous microstructures in some natural impure calcite (Frisia-Bruni and Wenk 1985; Gunderson and Wenk 1981; Wenk and Zhang 1985; Barber and Khan 1987; Khan and Barber 1990) but their relationship to the original surface microtopography could not be established. Surprisingly, given their complex morphology and compositional zoning, many synthetic and natural calcite crystals alike show a homogeneous microstructure (Reeder 1992a).

Dolomite presents a different challenge. Its nucleation and crystal growth are strongly inhibited at room temperature and, so far, successful precipitation of dolomite from a fluid or by replacement of a $CaCO_3$ precursor has only been produced experimentally near or at hydrothermal conditions (e.g., Lumsden et al. 1995; Sibley et al. 1994; Gaines 1980; Tribble et al. 1995). Hence, very few TEM observations exist of synthetic dolomites. On the other hand, TEM studies of natural sedimentary dolomites (particularly calcian dolomites) have copiously documented the preservation of complex microstructures but the conditions of formation of the host crystals are generally poorly constrained (Reeder 1981; Wenk et al. 1983; Barber et al. 1985; Meike et al. 1988; Van Tendeloo et al. 1985; Reksten 1990; Fouke and Reeder 1992; Frisia and Wenk 1993; Frisia 1994).

This paper evaluates the utility of two TEM techniques for calcite and dolomite, Pt-C replicas and ultramicrotomy, that bridge the gap between the conventional imaging of bulk microstructures in ion-milled foils and surface characterization by AFM. Both techniques were used previously on clay minerals (e.g., Baronnet 1992; Vali and Bachmann 1988; Vali and Hesse 1990; Vali et al. 1991). Pt-C replicas of as-grown surfaces provide a high-resolution, nearly three-dimensional image of surface topography (Skatulla and Horn 1960). By using Pt-C replicas on cleaved and as-grown surfaces, bulk microstructures can be compared to the surface microtography of crystals to determine whether or not the shape and scale of growth steps or islands on different crystallographic surfaces produce distinctive microstructures in the bulk crystal. Our interest in ultramicrotomy lies primarily in its potential for the study of crystals that are difficult and time-consuming to prepare by conventional ion-thinning. The main advantage of ultramicrotomy over conventional ion-thinning is that sections can be prepared more quickly and their whole area can be imaged rather than the very small ion-thinned portion studied on conventional foils. It can complement the Pt-C replica technique since ultrathin sections from single crystals can be analyzed at a near-nanometer scale by analytical electron microscopy (AEM). Because carbonate minerals cleave and twin readily under stress, new interfaces may be created during sample preparation and can potentially complicate the identification of original microstructures. To ascertain if features related to growth mechanisms are obscured by microcleavage and deformation twinning during sample preparation, the microstructures of natural dolomites imaged by TEM were compared with those of synthetic calcite grown from aqueous solutions under monitored conditions.

MATERIAL AND METHODS

Synthetic calcite

We examined synthetic single crystals of Mn/Sr/Pb-doped calcite (sample J-4 from Vaillancourt and Paquette 1995), a Mg/Mn-doped calcite (Paquette and Reeder 1995) and a Mn-doped calcite (ES-1). The crystals were grown at room temperature or slightly higher, to sizes of 300–500 μm, from NH_4Cl-$CaCl_2$-CO_3 aqueous solutions by a free-drift technique modified from Gruzensky (1967), described by Paquette and Reeder (1995), and summarized in Table 1.

Natural dolomite

Three dolomite cements were selected for this study from subsurface cores of Upper Devonian reef carbonates in the

TABLE 1. Summary of crystal composition and growth conditions for synthetic calcite

Sample	Dopant concentration in solution (ppm)	Soln. *T* (°C)	Ca molarity	NH_4Cl molarity	pH Range	Crystal chemistry (ppm)	Morphology	Zoning type
Mn/Mg-doped	Mg: 4 Mn:0.05	27	0.01	0.7	7.4–7.3	MgO: 75–400	{$10\bar{1}4$} dominant	intrasectoral
J-4	Pb: 10 Sr: 5 Mn: 0.03	27	0.05	1.0	7.8–7.5	PbO: 5000–50,000 SrO: 500–2000 MnO:100–1200	hopper {$10\bar{1}4$} dominant {$01\bar{1}2$}	intrasectoral; sectoral (slight)
ES-1	Mn: 0.05	27–38	0.1	1.4	7.3–7.1	MnO: 1000–2000 {$10\bar{1}4$}	{$01\bar{1}2$} dominant	oscillatory and intrasectoral

Western Canada Sedimentary Basin: a "planar-s(e)" burial dolomite (sample PR-1, Marquez 1994; type 2 of Mountjoy and Amthor 1994) from the Strachan buildup along the Rimbey-Meadowbrook reef trend; a saddle dolomite (sample SD-1) from the Middle Devonian Presqu'Ile Barrier (Qing and Mountjoy 1994), and a "planar-s(e)" shallow-burial dolomite (sample S104, Whittaker and Mountjoy, submitted; type 3 of Mountjoy and Amthor 1994) from the carbonate-evaporite system in the eastern shelf region of the Western Canada Sedimentary Basin.

PREPARATION TECHNIQUES

Single crystals of synthetic calcite were picked from the Tygon tubing used as a substrate during the growth experiment. Surface replicas were prepared from three types of surfaces: free as-grown surfaces (i.e., the former solution-crystal interface, Fig. 1a), surfaces grown against Tygon tubing (i.e., the former substrate-crystal interface, Fig. 1b) and cleaved surfaces (Figs. 1c and 1d). The cleaved surfaces were obtained by gently crushing single crystals with an agate pillar and mortar.

Fragments of carbonate rocks containing euhedral crystals of dolomite cements were separated with a knife under the stereomicroscope. The individual crystals were isolated by gently crushing the larger fragments in an agate mortar. Particles smaller than 30 μm were removed using a 32 mesh sieve. The remaining crystals were cleaned in a water-alcohol-mixture solution, immediately dried with pure alcohol and stored in a desiccator. Pt-C replicas were only prepared from cleaved surfaces because the original faces were clearly damaged.

Pt-C replica

The replicas consist of a thin Pt/C-metal film (1–2 nm thick; 95 wt% Pt, 5 wt% C) and a 15–20 nm thick supporting carbon film. The shadowing and replication of the specimens were performed at room temperature in a Balzer 400 freeze-etch unit under high vacuum (10^{-6} Torr). Fragments or whole crystals were mounted on double-sided sticky tape with the surface of interest oriented parallel to the stage. A Pt/C film was condensed on the crystal surface by an electron beam evaporation gun. Because the resolution of the replica depends on the thickness of the metal film, the latter was monitored using a quartz crystal thin-film oscillator mounted as close as possible to the specimen. A supporting carbon film was immediately condensed on the Pt/C coating. The replica, cleaned by dissolving the carbonate mineral with a 1% HCl solution, was transferred onto a 200-mesh Cu TEM grid.

Ultramicrotomy

Individual fragments showing euhedral faces were embedded in a low-viscosity resin (Spurr 1969) following the procedure described by Vali and Köster (1986). The embedding blocks were trimmed and ultrathin sections (70–80 nm thick) were cut with a LKB ultramicrotome and a Diatome diamond knife. A few ribbons consisting of 3–5 sections, oriented relative to crystal faces or edges, were selected from each specimen. They were transferred to conventional 200 or 300 mesh Cu TEM grids with a support film as a substrate. $CaCO_3$-saturated water was used as floating fluid to minimize dissolution during this operation. Unlike clay minerals (Vali and Hesse 1990), the crystal size of the carbonate minerals investigated was too large to allow for uniform impregnation by the resin. Thus ultrathin sections cut from crystals larger than 10 μm could not be kept whole and only fragments that were attached to the resin could be transferred to grids.

Instruments

TEM imaging, selected-area electron diffraction (SAED), and semi-quantitative analysis were performed using a JEOL 100 CX equipped with an energy-dispersive X-ray detector (PGT IV, analyzable area ~100 nm^2), operated at 100 kV with imaging conditions of underfocus (100–300 nm). A JEOL 2000, operated at 200 kV was used for high-resolution imaging.

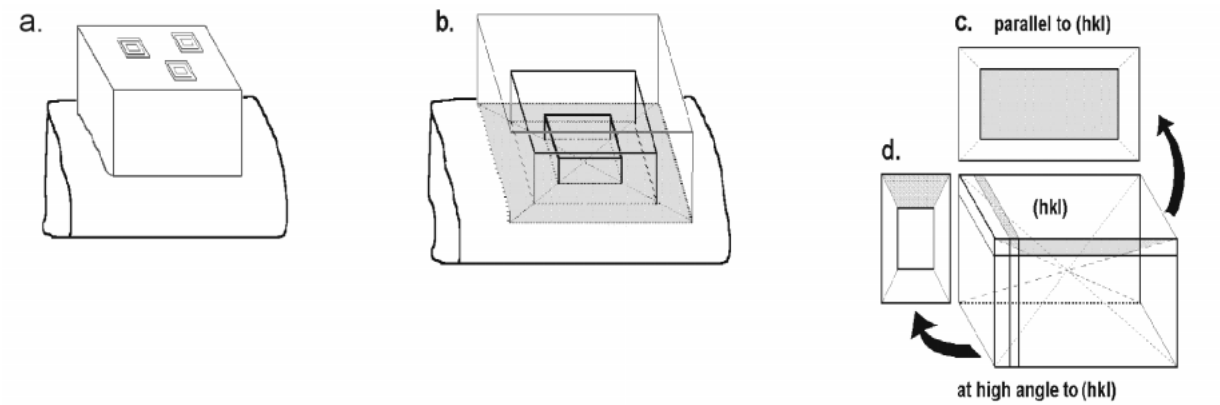

FIGURE 1. Schematic representation of the type of surfaces examined in this study. (**a**) The as-grown surface (shaded) represents the solution-crystal interface at the end of the crystal growth experiment. (**b**) The surface (shaded) grown against the Tygon tubing used as substrate displays a cross section through the internal zones of the crystal. (**c**) The microtopography of former growth surfaces can be seen in plan view (within the shaded area) on a slice parallel to the face in question. (**d**) A slice cut at high angle to a given face displays a cross section (shaded area) through the corresponding growth sector. Dotted lines indicate idealized growth sector boundaries.

Image interpretation

The high resolution replicas imaged by TEM were obtained by oblique evaporation of Pt/C (shadowing) onto the fresh surfaces of fragments cleaved from single crystals. The "shadowing" technique relies on the assumption that the local thickness of the replica corresponds to the depositional rate of the evaporated metal. Thus, the enhanced contrast observed in TEM images the surface topography of the specimen. However, surfaces with very low relief, and therefore a poor shadowing effect, commonly show a decoration pattern as a side effect of Pt shadowing. In such cases, decoration can enhance details of the surface structure.On the Pt/C replicas presented here, decoration typically appears as a granular pattern and indicates the formation of Pt clusters resulting from the preferential deposition of Pt atoms at sites with higher binding energy. The surface mobility of the Pt atoms on smooth crystal surfaces is responsible for the granularity and decoration pattern in replicas. Decoration is very sensitive to the chemical and structural composition of the surface and its detailed interpretation requires that rigorous experiments be performed. This was not our goal.

In most cases, TEM images obtained from the shadowing replica contain both negative (depressions) and positive (topographically high) features. A positive feature shows deposition of Pt atoms as a black rim facing the shadowing direction (indicated on images by an arrow) and a white "shadow" on the opposite side. On negative features the position of Pt accumulation and shadow are reversed with respect to the shadowing direction. Note that the TEM image of a shadowing replica is a projection onto a flat thin film. The true dimension and shape of a feature strongly depend on the exact orientation of the surface area of interest to the shadowing angle.

RESULTS

Synthetic calcite

Ideally, relating internal microstructures to the surface microtopography should be done by comparing matching pairs of replicas from each type of calcite: the first one prepared from an as-grown face (Fig. 1a), and the second from a section at high angle to the face in question (Fig. 1d). This was not always possible. In fact, replicas were most easily recovered from the relatively large and nearly smooth crystal surfaces grown against the substrate (Fig. 1b). These displayed a cross-section of the internal structure on which growth sectors corresponding to adjacent crystal faces could be easily indexed. The microstructures were strikingly different in crystals grown from different solutions and, within any single crystal, they changed in orientation or disappeared sharply across growth sector boundaries.

Mg/Mn-doped crystals. The replica from an as-grown ($10\bar{1}4$) face showed a large number of small, four-sided growth hillocks, with summits 0.1 to 0.5 mm apart (Fig. 2a). Two of the four vicinal faces on each hillock showed relatively straight steps while the opposite vicinals were smaller and less sharply defined. Many of these hillocks were aligned as if they were following the aretes or the edges of larger ones (Fig. 2b). Cross sections through corresponding {$10\bar{1}4$} sectors were homogeneous and showed no distinctive microstructure.

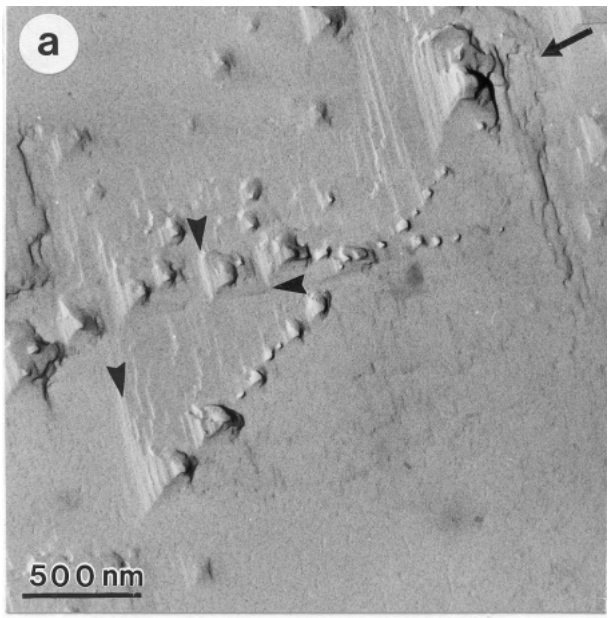

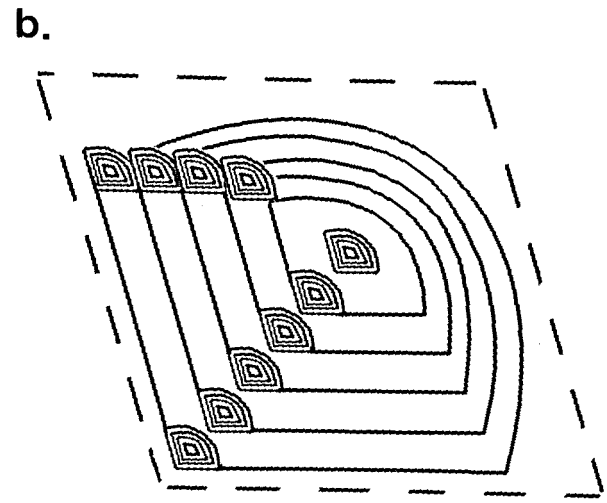

FIGURE 2. (**a**) TEM image from Pt-C replica of a Mg/Mn-doped single crystal of synthetic calcite. The replica is from an as-grown ($10\bar{1}4$) face. Numerous growth hillocks with four asymmetric vicinal faces are present, many of them aligned. The arrow in upper right corner indicates the direction of Pt shadowing. Steps (arrowheads) are more distinct on the larger vicinals of the hillocks. Scale bar = 0.5 μm. (**b**) Schematic diagram of growth hillock on a ($10\bar{1}4$) face showing vicinal faces formed by non-equivalent steps spreading toward the edges of the ($10\bar{1}4$) face (dashed outline). The steps spreading northward and eastward are slightly rounded. Similar smaller hillocks nucleate along the contact between vicinal faces. Orientation is similar that of Figure 2a but rotated 135° counterclockwise relative to Figure 9.

Mn/Sr/Pb-doped calcite (J4). Cathodoluminescence microscopy (CL) showed that growth hillocks were present in $\{10\bar{1}4\}$ sectors. Under the light microscope, the typical surface topography of $\{01\bar{1}2\}$ sectors consisted of triangular facets bounded by macrosteps (Fig. 8 in Paquette and Reeder 1995). Only fragments of replicas were recovered from as-grown faces on the $\{10\bar{1}4\}$ and $\{01\bar{1}2\}$ rhombohedra and they could not be oriented with certainty relative to the original faces. TEM observations were therefore made mostly from surfaces grown against the substrate (Figs. 3a–b) or cleaved (Fig. 3c). The $\{10\bar{1}4\}$ sectors showed a nearly uniform microstructure (Fig. 3a) but $\{01\bar{1}2\}$ sectors had a complex zonation (Figs. 3a and 3b). Throughout $\{01\bar{1}2\}$ sectors, wide bands containing striations alternated with thinner bands showing a uniform microstructure (Fig. 3b). Some crystals were crushed gently to see if any of these features might be recognizable on their freshly cleaved surfaces. There again, wide bands with a fainter pattern of S-shaped striations alternated with thinner bands showing a less distinct microstructure (Fig. 3c). Differential shadowing of the cleaved surface by Pt gave rise to lighter and darker bands (Fig. 3c), revealing that adjacent bands presented different slopes relative to the shadowing direction. It is not clear whether this slight tilt is a primary feature or if it reflects a slight deformation of the crystal during crushing. In any case, it did not hide an overall pattern of striations similar to that seen in intact crystals.

Mn-doped crystals (ES-1). The as-grown faces of these crystals were inadvertently etched during the last stage of the growth experiments and therefore their Pt-C replicas showed no distinct microstructures. Thin sections of these crystals examined by CL microscopy showed intrasectoral zoning and a very fine-scale oscillatory banding that could barely be resolved. TEM replicas of surfaces grown against the substrate showed an even finer-scale banding, 0.3–1 μm thick (Fig. 4a) in $\{10\bar{1}4\}$ sectors. The sharp interface between adjacent bands commonly widened laterally into a thin zone with a chaotic, granular microstructure (Fig. 4b). The banding showed a slight wavy curvature (Fig. 4a) that changed sharply in orientation at any growth sector boundary. Small, striated sectors seen along ramp-like features may represent facets developed at the edge of bunched layers (Fig. 4b). The only features that did not show any preferred orientation were the vague pockmarks scattered uniformly across the surface, which are likely to be masks of small irregularities on the Tygon tubing used as substrate.

Sedimentary dolomite cements

Saddle dolomite. The Pt-C replica from a cleaved surface parallel to a $(10\bar{1}4)$ face (as in Fig. 1c) showed an array of sharp, three-faced hillocks (Fig. 5a). The hillocks were consistently asymmetric, with two steeper faces and a third one more gently inclined. The surface exposed by cleaving at high angle

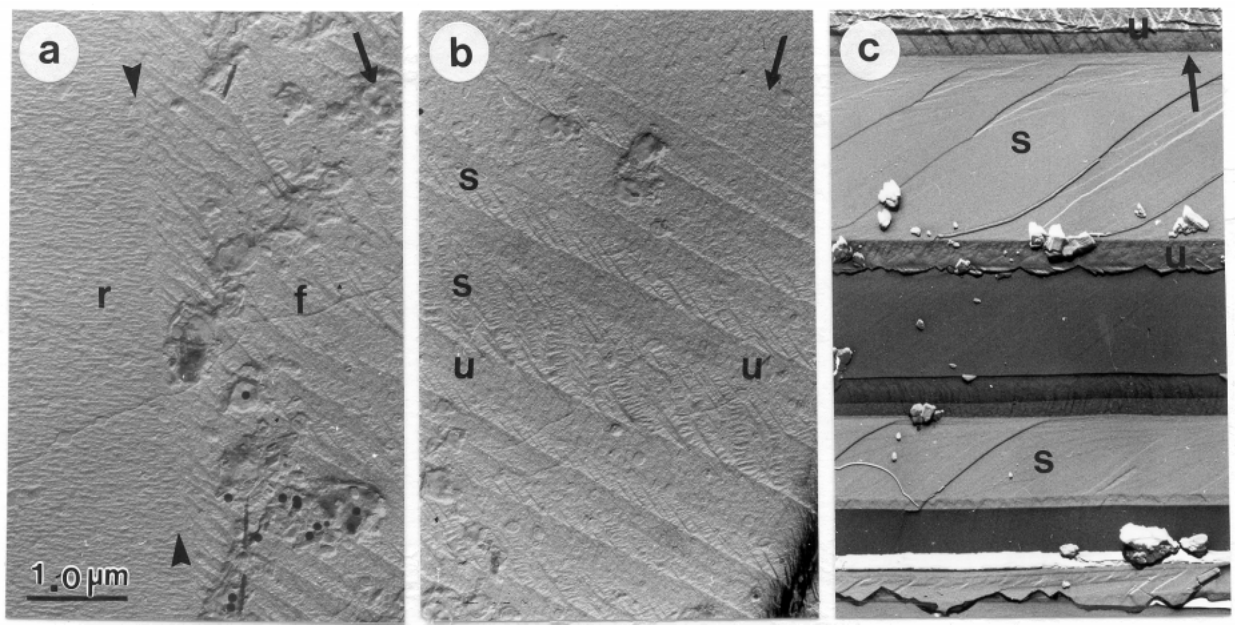

FIGURE 3. TEM images from a Pt-C replica of a Mn/Sr/Pb-doped single crystal of synthetic calcite. Arrow in upper right corner indicates the direction of Pt shadowing. Scale bar = 1 μm. (**a**) The surface replicated grew against the Tygon tubing used as substrate during calcite precipitation. To the left, a $10\bar{1}4$ sector (**r**) shows a uniform microstructure. A sharp growth sector boundary (arrowheads) separates it from the $01\bar{1}2$ sector (**f**) to the right. Inclusions of a second phase are abundant in the $01\bar{1}2$ sectors near the contact between the two sectors. (**b**) Different area from same replica as (**a**). The $01\bar{1}2$ sector shows alternating bands with different microstructures: wider bands (**s**) contain regularly spaced S-shaped striations and the thinner bands (**u**) are uniform. (**c**) Replica from a cleavage face at high angle to a $01\bar{1}2$ sector. Faintly striated bands (**s**) alternate with thinner uniform ones. The orientation of the striations is reversed relative to those in (**a**) and (**b**). Intensity contrasts among bands indicate that their surfaces were slightly tilted toward or away from the shadowing direction, probably by deformation twinning along $\{01\bar{1}2\}$ and at interfaces separating **s** and **u** bands.

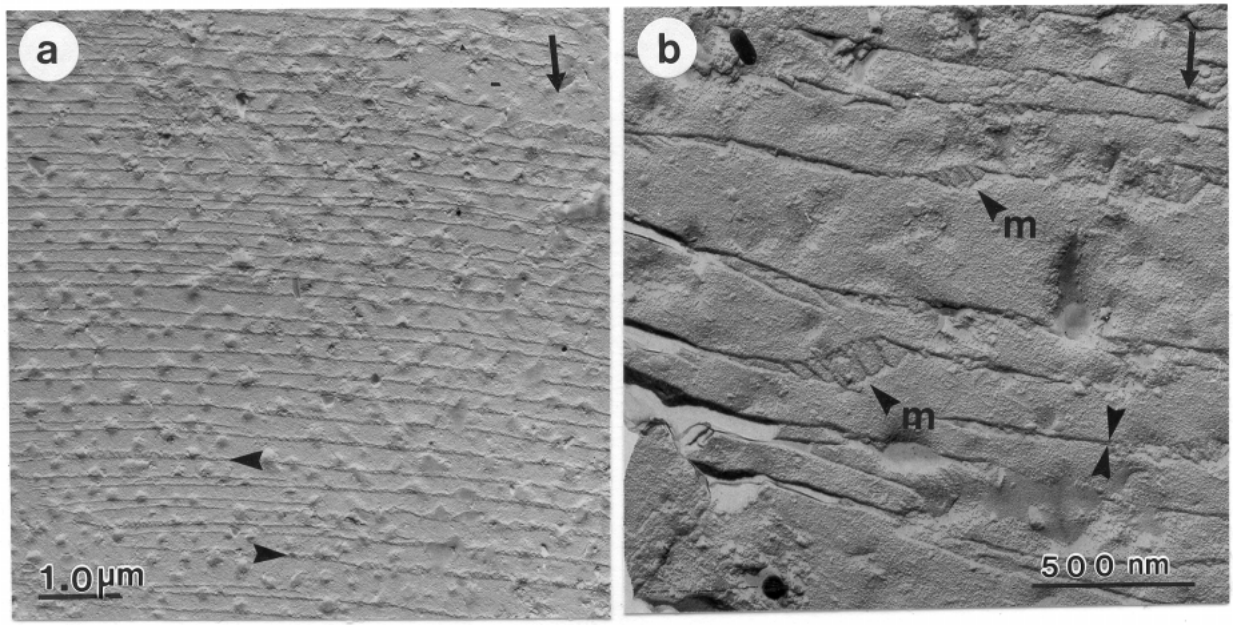

FIGURE 4. TEM images from the Pt-C replica of an oscillatory-zoned Mn-doped single crystal of synthetic calcite. The surface replicated grew against the substrate and displays a section at high angle to the $10\bar{1}4$ sector. Arrow in upper right corner indicates the direction of Pt shadowing. (**a**) Fine-scale banding is visible and shows lateral transitions to thin, roughened zones (arrowheads). Its slight curvature may be due to slight topographic relief on large hillocks. The pockmarks are small depressions on the original calcite surface grown against tiny bumps on the substrate. Scale bar = 1 µm. (**b**) Detail from the same surface. A double arrow points to a sharp interface that widens laterally into thin rougher zones. Small sectors (**m**) showing steps are also visible against the edge of ramps. Scale bar = 0.5 µm.

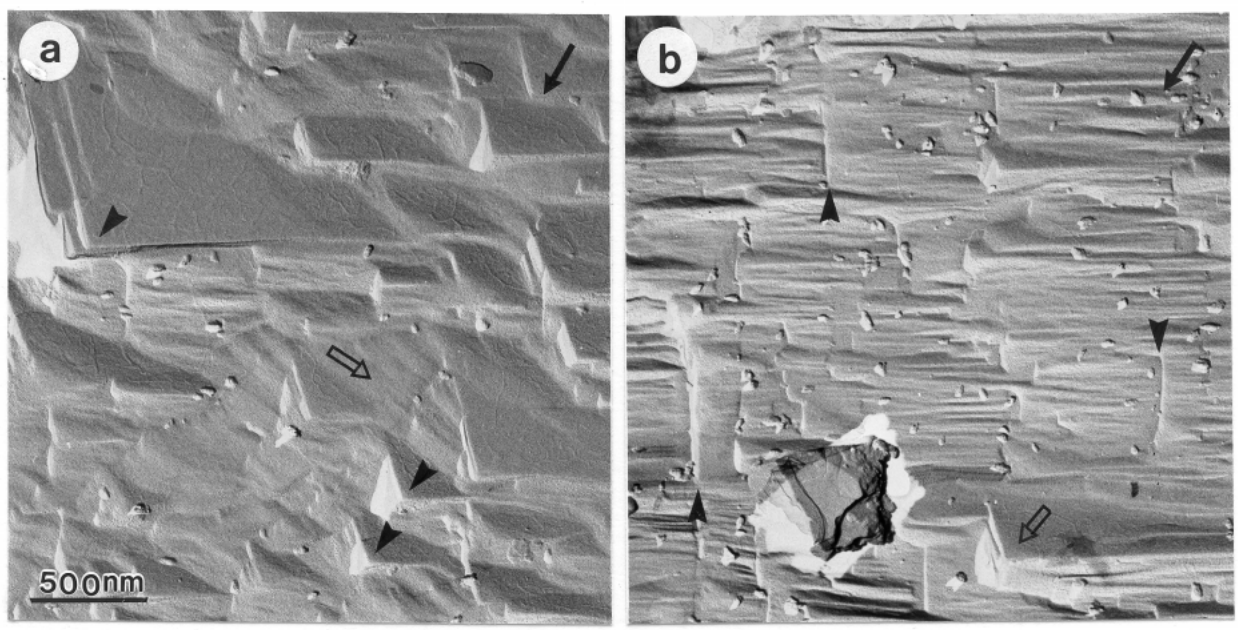

FIGURE 5. TEM images from Pt-C replicas of a natural saddle dolomite (SD-1). Arrow in upper right corner indicates the direction of Pt shadowing. (**a**) Freshly cleaved surface parallel to a $(10\bar{1}4)$ face. Black arrowheads point to some asymmetric hillocks consisting of two light-colored, narrow, vicinal faces and a larger darker one sloping more gently toward the Pt shadowing direction. Fainter steps trending NW-SE are visible between the hillocks (open arrow). (**b**) Surface exposed by cleaving at high angle to a $(10\bar{1}4)$ face. A faint, diffuse subhorizontal banding is interrupted at perpendicular boundaries (vertical arrowheads). A large hillock is visible in the lower right corner (open arrow).

to a $(10\bar{1}4)$ face showed a faint, diffuse, fine-scale banding. These faint features were interrupted by many discontinuous high-angle boundaries (Fig. 5b) with an average spacing similar to that of hillocks seen in the face-parallel section (Fig. 5a). Scattered three-sided hillock-like features also poked through the surface (Fig. 5b).

Planar-s(e) dolomite (PR-1). The crystals consisted of cloudy, euhedral $\{10\bar{1}4\}$ rhombohedra with limpid outer rims. Replicas and ultrathin sections were prepared from the outermost rim. The Pt-C replica from a surface freshly cleaved parallel to a $(10\bar{1}4)$ face showed no hillocks and its smooth surface was modified by two types of non-equivalent facets (labeled v and f in Fig. 6a). The section at high angle to a $(10\bar{1}4)$ face (Fig. 6b) showed sharp fine-scale banding crosscut by sharp boundaries. These boundaries were larger features than in the saddle dolomite (Fig. 5b) and formed distinct aretes between two sloping surfaces. On one side of each boundary a narrow flank was strongly shadowed (white on Fig. 6b), masking any detail within it. In a few areas, the banding showed a slight break in slope. Toward the edges of the section, areas of fine-scale banding were often intercalated with domains showing a homogeneous microstructure (Fig. 6b).

Ultrathin sections of this dolomite were also prepared (Fig. 7a). A lamellar structure, superficially similar to the fine-scale banding seen in the Pt-C replica (Fig. 6b) was found parallel to the original $(10\bar{1}4)$ face. The crystal was clearly disrupted locally, especially at the edges of ultrathin sections and some sections showed tearing (Fig. 7). Nevertheless large areas appeared to remain coherent. Within these, the ends of successive lamellae were often aligned along a boundary nearly perpendicular to the lamellar structure (Fig. 7a). Individual bands often showed slight changes in thickness and orientation, sometimes giving rise to sharp ramps. These were often found next to lenticular domains (Fig. 7a) into which the banding of the host sector could not be traced.

Because of the perfect cleavage of rhombohedral carbonate minerals, it is possible that the lamellar structure seen in ultrathin section is a preparation artifact induced by ultramicrotomy. To evaluate this, ultrathin sections were prepared from other natural dolomites as well as synthetic and natural calcite. In dolomite S$10\bar{1}4$ (Fig. 7b), disruption occurred along *two* directions consistent with the orientation of symmetry-equivalent cleavage planes. In this dolomite (and several others), this pervasive microcleavage did not mask a dominant lamellar structure parallel to the $(10\bar{1}4)$ crystal face which may have followed an original microstructure. Disruption was less regular along the high-angle direction, showing many small offsets (Fig. 7b). Natural and synthetic calcite treated by ultramicrotomy showed much more pronounced disruption than any of the dolomite, obliterating any original microstructure.

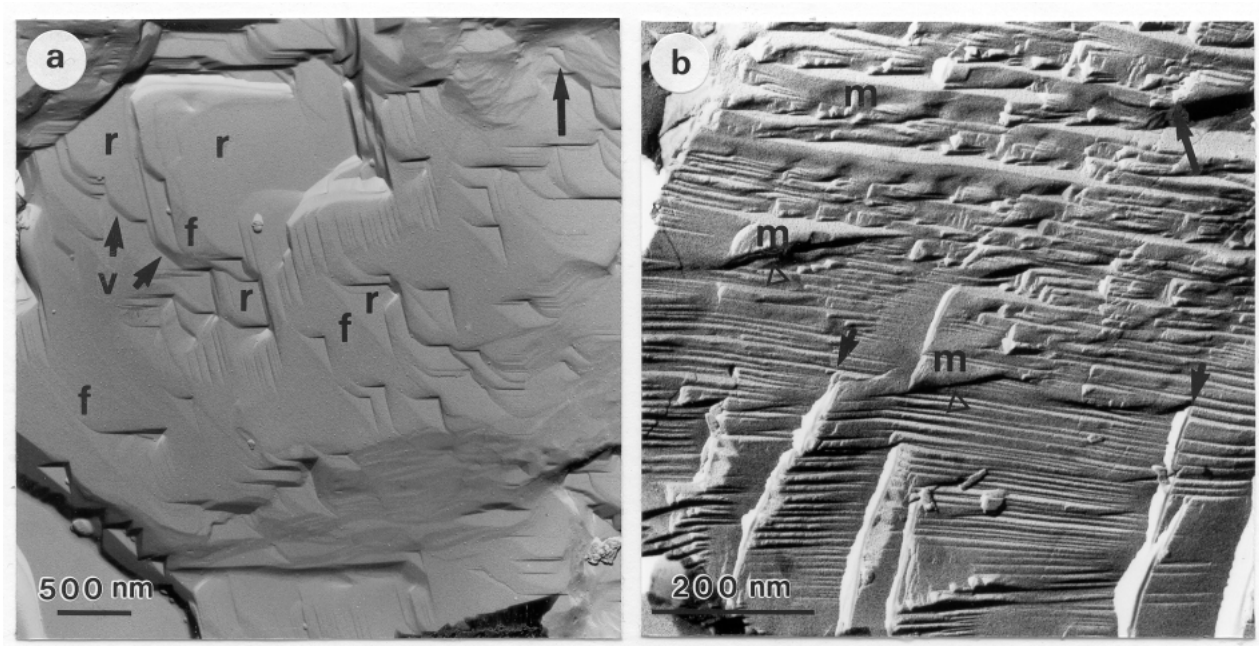

FIGURE 6. TEM images from Pt-C replicas of a planar-s(e) dolomite (PR-1). Arrow in upper right corner indicates the direction of Pt shadowing. Scale bar = 0.5 μm. (**a**) Surface cleaved parallel to a former $(10\bar{1}4)$ face. Two types of non-equivalent facets (**f**, **v**) are present in addition to the dominant $(10\bar{1}44)$ face (**r**). (**b**) Surface exposed by cleaving at high angle to a former $(10\bar{1}4)$ face. Scale bar = 0.2 μm. The sharp, horizontal, fine-scale banding is commonly interrupted at nearly perpendicular boundaries (arrowheads pointing downward). A narrow subsector (white) may lie to the right of same boundaries, but its internal microstructure is masked by shadowing. Some breaks in slope (arrowheads pointing upward) may correspond to the contact between non-equivalent vicinal faces of a growth hillock (Fig. 9). Other domains (**m**) show no banding.

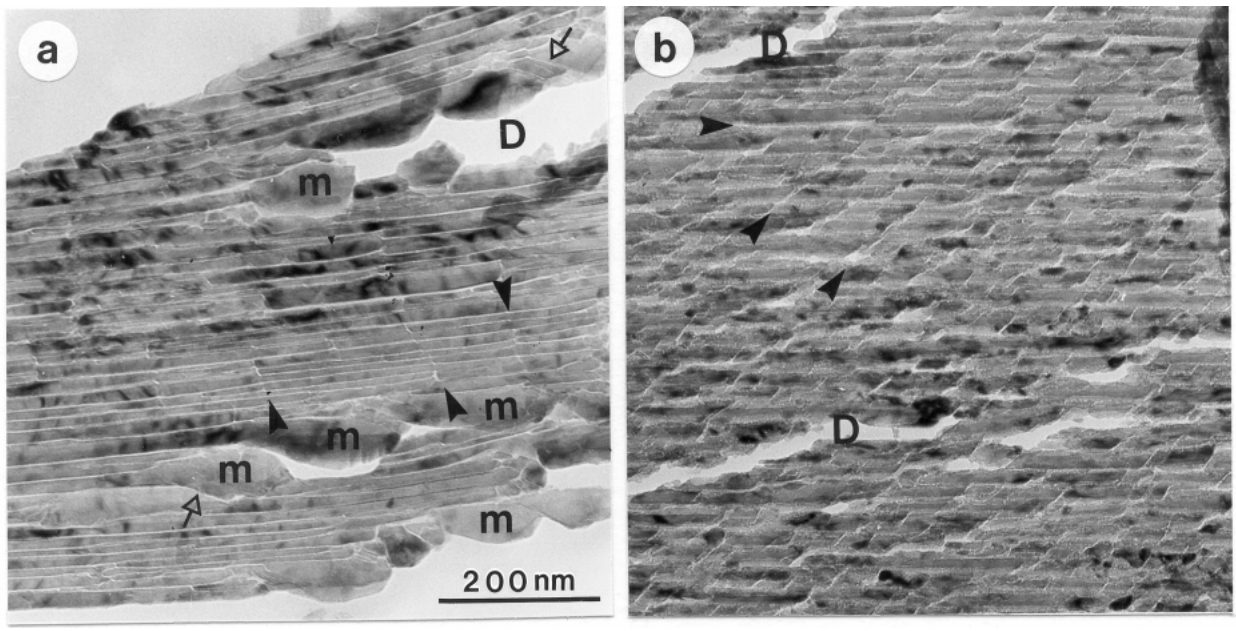

FIGURE 7. TEM images of ultrathin sections from planar-s(e) dolomites. White areas due to disruption (**D**) of the sections are preparation artifacts. Scale bar = 200 nm (0.2 μm). (**a**) Planar-s(e) dolomite PR-1. The lamellar structure is commonly interrupted by nearly perpendicular boundaries (full arrowheads) where adjacent lamellae meet against each other. Sharp ramps (open arrowheads) are often found next to massive domains (**m**). (**b**) Planar-s(e) dolomite S101–4. Pervasive disruption occurred along two directions (arrows) consistent with the orientation of symmetry-equivalent $\{10\bar{1}4\}$ cleavage planes. In these images the contrast at the interface between adjacent lamellae was enhanced by the imaging conditions in TEM (100 kV, 200–300 nm underfocus).

DISCUSSION

Growth hillocks on $\{10\bar{1}4\}$

Growth hillocks diagnostic of a spiral growth mechanism, are ubiquitous on the faces of the $\{10\bar{1}4\}$ rhombohedron in synthetic calcite crystals grown from aqueous solutions. At low to moderate supersaturation states, single hillocks commonly spread laterally for hundreds of micrometers but may rise less than five micrometers above the crystal surface (Paquette and Reeder 1990, 1995; Staudt et al. 1994). Their large area and low relief make them difficult to identify by scanning electron microscopy (SEM) or TEM since the field of view covers a very small area of the crystal surface. It is not surprising, therefore, that large hillocks would be elusive features. All our synthetic calcites examined by CL microscopy showed $\{10\bar{1}4\}$ sectors containing intrasectoral zoning, an indication that layer-by-layer growth took place on relatively large spirals where differential incorporation of Mn took place at non-equivalent steps (e.g., Fig. 2b in Paquette and Reeder 1990). The only growth hillocks we could image by TEM were those less than 1 μm across, on the surface of the Mn/Mg-doped calcite, and these were far and few between. The other two calcite crystals also showed evidence of spiral growth by CL microscopy, but high-angle sections through $\{10\bar{1}4\}$ sectors (Figs. 3a and 4a) revealed no distinctive microstructure that could be related unequivocally to these large growth hillocks.

The features observed on fragments cleaved parallel to a $(10\bar{1}4)$ surface (as in Fig. 1c) of the two diagenetic dolomites examined suggest that former growth surfaces were uncovered. The three-sided shallow pyramids visible on a cleaved surface of a saddle dolomite (Fig. 5a) are similar to the larger asymmetric growth spirals seen on faces of the $\{10\bar{1}4\}$ rhombohedron in synthetic calcite (e.g., Fig. 4C in Paquette and Reeder 1990) but the lack of sharp steps on their flanks makes this interpretation tentative. Growth taking place dominantly on the less distinct steps between the hillocks, parallel to <010>, could have been a factor in the development of non-planar surfaces since faces dominated by a single set of parallel steps tend to develop rounding at higher growth rates (Sunagawa 1987). The few hillock-like features poking through the vague banding visible in the high-angle section (Fig. 5a), suggest a strongly stepped surface microtopography.

Elementary steps are also missing on the smooth surfaces and facets (Fig. 6a) uncovered by cleaving the planar-s(e) dolomite cement (PR-1) parallel to a $(10\bar{1}4)$ face. But the slight changes in slope of the banding visible in the high-angle section (Fig. 6b) might reflect the profile of vicinal faces on growth spirals (Fig. 8) and would be consistent with the subdued surface topography seen in Figure 6a.

The banding in the planar-s(e) dolomite (Fig. 6b) consists of zones 30–150 nm thick, and it is in the range (7.5–1000 nm) reported from other TEM studies (Reeder and Prosky 1986; Ward and Reeder 1993; Fouke and Reeder 1993). If this banding can reasonably be interpreted as growth banding, the nature of the high-angle boundaries that interrupt it is more problematic. Similar sharp perpendicular discontinuities interrupt the less distinct banding seen in the saddle dolomite (Fig. 5b). Their orientation is not compatible with cleavage or a fracture pattern but is similar to that of dislocations imaged by conventional TEM. Because their spacing is the same as that of

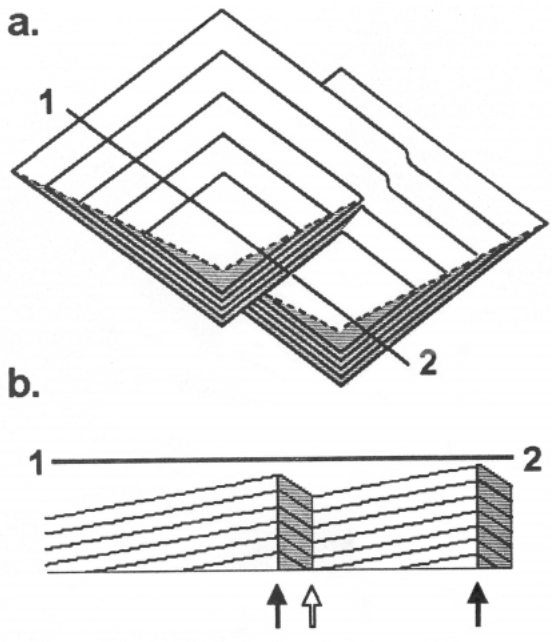

FIGURE 8. (**a**) Schematic plan view of two hillocks on which layers spread in opposite directions at different rates. Shaded portion shows the subsectors or vicinal faces formed by the more slowly spreading steps. (**b**) Schematic cross section through the same hillocks with vertical scale greatly exaggerated, showing how concentric growth banding may preserve evidence of the former growth microtopography. If intrasectoral zoning is present, compositional interfaces will crosscut this banding at the contact between vicinal faces, within a single hillock (black arrows) and between adjacent hillocks (white arrow).

growth hillocks (Fig. 5a) they may represent the interface between non-equivalent, asymmetric subsectors within single hillocks, or the contact along which layers met as they grew on the non-equivalent vicinal faces of adjacent hillocks (Fig. 8). In doped synthetic calcite, either type of contact corresponds to a sharp change in composition, often imaged at a larger scale by CL microscopy in Mn-doped crystals (e.g., Paquette and Reeder 1990; Paquette et al. 1993). The second possibility is perhaps more likely because layers growing on adjacent hillocks may join with a slight mismatch and give rise to local defects.

Microstructure of {01$\bar{1}$2} sectors in synthetic calcite

The striations in the wider concentric zones (s in Fig. 3c) are characteristic of growth on sectors developed on facets formed by the bunching of elementary growth layers. The striations represent non-equivalent subsectors within the host {01$\bar{1}$2} sector. Analogous but larger subsectors grown on macrosteps within {10$\bar{1}$4} sectors were identified before in synthetic calcite (Paquette et al. 1993) and natural dolomite (Fouke and Reeder 1992) where they were likened to the type II striations observed by Bauser and Strunk (1984) in semiconductors.

The remarkably regular spacing of the striations (Fig. 3b) is consistent with a surface consisting of a mosaic of facets and terraces nearly uniform in size and covering large areas of a single crystal face. The sigmoidal shape of the striations (more distinct in Fig. 3c) suggests that the variations in the relative growth rates of the facets and the host sector were remarkably cyclical throughout the whole sector. The succession of broad striated bands and thinner quasi-uniform ones suggests that two distinct growth mechanisms were alternating in {01$\bar{1}$2} sectors but not in the adjacent {10$\bar{1}$4} sectors where the microstructure is uniform.

Sectors of forms other than {10$\bar{1}$4} in dolomite

The domains (labeled m in Figs. 6b, 7a) intercalated within the banded {10$\bar{1}$4} sectors are interpreted as non-equivalent sectors grown on the f facets seen on the larger (10$\bar{1}$4) face (Fig. 6a). They are an example of sectors grown on facets similar, though not necessarily crystallographically equivalent, to those described by Fouke and Reeder (1992). These authors noted, as we do, that the pervasive fine-scale banding of {10$\bar{1}$4} sectors could not be traced into such non-equivalent sectors, suggesting that different growth mechanisms prevailed in each type of sector.

Oscillatory zoning

The Mn-doped synthetic calcite (ES-1, Fig. 4), oscillatory-zoned under CL, was the only synthetic calcite examined where cross sections through {10$\bar{1}$4} sectors showed concentric fine-scale banding. The boundaries defining this banding vary laterally from knife sharp interfaces to areas where they thicken and roughen along individual bands. This texture was not seen on the back side of synthetic calcite crystals grown on the same substrate but at a lower supersaturation, and is it therefore unlikely to be a mask of features on the Tygon tubing. This raises the possibility that periodic changes in microtopography may accompany the development of compositional oscillatory zoning. In magnesian calcite grown from highly supersaturated solutions, a patchwork of growth islands often grades into smoother overgrowths over a single face 2–4 mm across (Fig. 6 in Paquette et al. 1996). In high-angle sections, such transitions could look very much like those seen in Figure 4. Dove and Hochella (1993) documented the case, in moderately supersaturated aqueous solutions, where growth on the (10$\bar{1}$4) face of a calcite crystal started by 2DNG and gave way to spiral growth within 2 hrs. If periodic but transient episodes of surface nucleation were typical of oscillatory zoning, it might be difficult to catch them in real time by AFM experiments. The evolution of microtopography over a large surface area may be much easier to document by looking for the resulting microstructure preserved on the surface grown against the substrate or on surfaces cleaved through a growth sector.

Can the fine-scale banding seen in the planar-s(e) dolomite (Figs. 6b and 7a) have a similar origin? The fact that this banding could not be traced into non-equivalent sectors within {10$\bar{1}$4} host sectors suggests that it is related to a face-specific growth mechanism rather than a change in bulk fluid properties. In our synthetic calcites, periodic changes in growth mechanism produced fine-scale banding in {10$\bar{1}$4} sectors of ES-1 crystals (Fig. 4). In the J4 calcite, on the other hand, only {01$\bar{1}$2} sectors were affected (Fig. 3a). Similar variations can be expected among non-equivalent growth sectors in dolomite.

Comparisons with conventional TEM images

Conventional TEM images obtained by the transmission of electrons through an ion-thinned foil reflect contrasts in strain

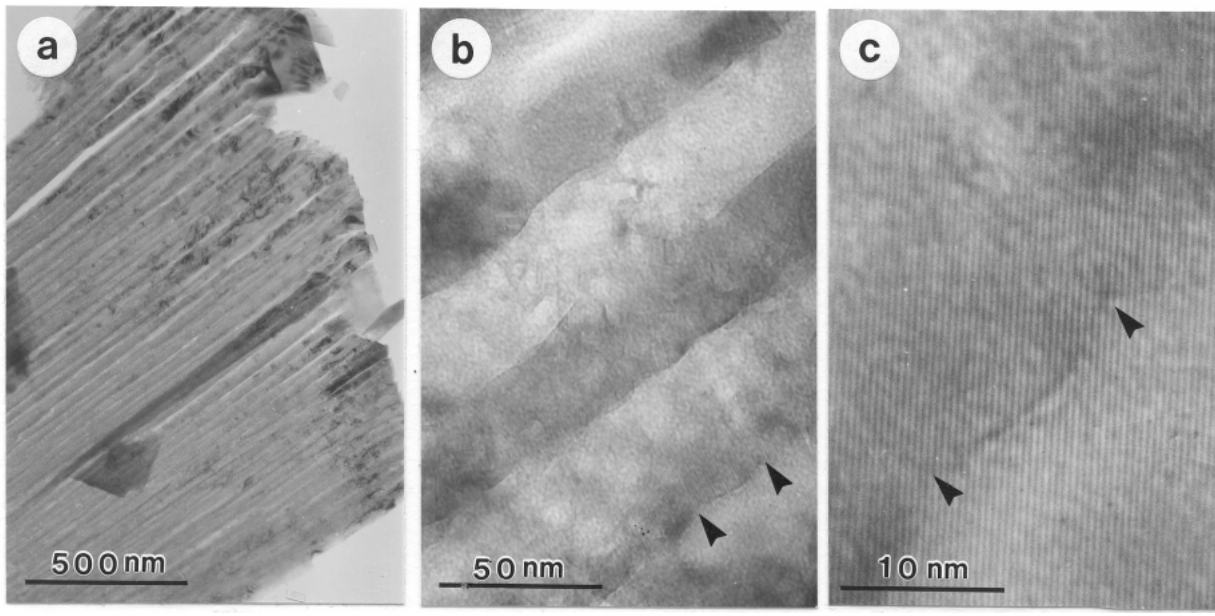

FIGURE 9. High-resolution TEM images, at 200 kV and near-scherzerfocus, of an ultrathin section of the planar-s(e) dolomite PR-1. (**a**) Lamellar structure, diffuse because of imaging conditions. Scale bar = 500 nm. (**b**) Detail of the lamellar structure seen in (**a**) with arrowheads pointing to an interface between lamellae. Scale bar = 50 nm. (**c**) Closeup view, arrowheads in same position as in (**b**) where lattice fringes show no disruption within the plane of the image. Scale bar = 10 nm.

and/or composition in the bulk crystal (Wenk et al. 1983). Pt shadowing reveals primarily the surface microtopography and, in this respect, the resulting images are more akin to those obtained by SEM. We expected that slight irregularities during their growth process would impart distinctive topographic features to as-grown surfaces of non-equivalent sectors. It is puzzling but promising that these features can also be imaged on freshly cleaved surfaces and on surfaces grown against a substrate (Fig. 3). Comparisons of Pt-C replicas and conventional TEM images from ion-thinned foils of synthetic single crystals could help determine which microstructures (e.g., Ca-rich ribbons and modulated structure) and defects (e.g., dislocation loops) relate directly to the steps defining the surface microtopography.

Ultrathin sections show that the high shear strain involved in slicing the crystal produces disruption that may obscure original microstructures (Fig. 7b). Calcite appears to be particularly vulnerable to this type of damage but dolomite is less disrupted. The lamellar structure in the dolomite of Figures 7a, 9a appears to follow original growth banding and does not mask non-equivalent sectors and ramps that are also visible on Pt-C replicas (Fig, 6b). In this case, high-resolution TEM shows no evidence of lattice disruption at the interfaces boundary of the individual lamellae in ultrathin section (Figs. 9b and 9c). An approach combining ultrathin sections and Pt-C replicas could provide a useful complement to conventional TEM studies of dolomite if ultramicrotomy is used cautiously.

Implications and future work

Dolomite is not as diverse in its external morphology as calcite, at least macroscopically, and it shows peculiar, but common, variations such as saddle dolomite. These differences and contrasts in their respective microstructures and precipitation kinetics, have led some to suggest alternatives to a dislocation-controlled layer-by-layer growth mechanism for calcian dolomite (e.g., Gregg and Sibley 1984; Barber et al. 1985; Reksten 1990). Our TEM observations suggest that spiral growth operating at different scales, and possibly alternating with episodic surface nucleation, creates some of the microstructures seen in calcite and dolomite $\{10\bar{1}4\}$ rhombohedra. Variations in scale alone of growth spirals could explain notable differences among synthetic and natural carbonate minerals. Compositional intrasectoral zoning, invariably associated with growth spirals in synthetic calcite doped with foreign ions, is apparently scarce in natural calcite and scarcer still in dolomite (Reeder 1992b). But if growth takes place on a large number of much smaller spirals, the resulting zoning may simply go undetected by backscattered electron imaging or CL microscopy. The extensive development of non-equivalent facets on {1014} of the planar-s(e) dolomite also suggests that compositional sectoral zoning may be present in dolomite crystals that appear as euhedral rhombohedra under the light microscope.

The possibility that growth on $\{10\bar{1}4\}$ operates by a dislocation-controlled spiral mechanism similar to that of calcite has other implications for our understanding of sedimentary dolomites. In synthetic calcite, the shape, size, and number of growth hillocks are highly sensitive to pH, the saturation state of the parent solution, and the presence of foreign ions or compounds (Paquette and Reeder 1995; Paquette et al. 1996; Teng et al. 1998). Environmental factors probably also control the range of microstructures found in natural dolomites. Until experimental work provides a basis for their interpretation, the

description of microstructures could be helpful in correlating or discriminating among types of dolomite that are otherwise very similar under the optical microscope.

ACKNOWLEDGMENTS

This work was supported by an FCAR grant (Programme Nouveaux Chercheurs) to Paquette, NSERC operating and strategic grants to Paquette and Mountjoy and a grant from the Petroleum Research Fund of the American Chemical Society. We acknowledge the generosity of M.F. Lalli for access to the transmission electron microscope and sample preparation facilities at the department of Anatomy and Cell Biology of McGill University. We are also indebted to Maria Espinosa and Nathalie Fagnan, who monitored the crystal growth experiments, and to Glenn Poirier who assisted with the compositional mapping of the synthetic calcite. Comments by Al Mucci on an earlier version helped improve the manuscript, as did reviews by Gordon Nord, Patricia Dove, Rich Reeder, and one anonymous reviewer.

REFERENCES CITED

Barber, D.J. and Khan, M.R. (1987) Composition-induced microstructures in rhombohedral carbonates. Mineralogical Magazine, 51, 71–86.

Barber, D.J., Reeder, R.J., and Smith, D.J. (1985) A TEM microstructural study of dolomite with curved faces (saddle dolomite). Contributions to Mineralogy and Petrology, 91, 82–92.

Baronnet, A. (1992) Polytypism and stacking disorder. In Mineralogical Society of America Reviews in Mineralogy, 27, 231–288.

Bauser, E. and Strunk, H.P. (1984) Microscopic growth mechanisms of semiconductor: Experiments and models. Journal of Crystal Growth, 69, 561–580.

Bosbach, D. and Rammensee, W. (1994) In situ investigation of growth and dissolution on the (010) surface of gypsum by Scanning Force Microscopy. Geochimica et Cosmochimica Acta 58, 843–849.

Dove, P.M. and Hochella, M.F. Jr. (1993) Calcite precipitation mechanisms and inhibition by orthophosphate: In situ observations by scanning force microscopy. Geochimica et Cosmochimica Acta, 57, 705–714.

Fouke, B.W. and Reeder, R.J. (1992) Surface structural controls on dolomite composition: evidence from sector zoning. Geochimica et Cosmochimica Acta, 56, 4015–4024.

Frisia-Bruni, S. and Wenk, H.-R. (1985) Replacement of aragonite by calcite in sediments from the San Cassiano Formation (Italy). Journal of Sedimentary Petrology, 55, 159–170.

Frisia, S. and Wenk, H.-R. (1993) TEM and AEM study of pervasive, multi-step dolomitization of the Upper Triassic Dolomia Principale (northern Italy). Journal of Sedimentary Petrology, 63, 101–49–1058.

Frisia, S. (1994) Mechanisms of complete dolomitization in a carbonate shelf: comparison between the Norian Dolomia Principale (Italy) and the Holocene of Abu Dhabi Sabkha. In B. Purser, M. Tucker, and D. Zenger, Eds. Dolomites: a volume in honour of Dolomieu. Special Publication of the International Association of Sedimentologists, 21, 55–74.

Gaines, A.M. (1980) Dolomitization kinetics: Recent experimental studies. In D.H. Zenger, J.B. Dunham and R.L. Ethington, Eds., Concepts and Models of Dolomitization. Society of Economic Paleontologists and Mineralogists Special Publication, 28, 81–86.

Goldsmith, J.R. and Graf, D.L. (1958) Structural and compositional variations in some natural dolomites. Journal of Geology, 66, 678–693.

Gratz, A.J., Hillner, P.E., and Hansma, P.K. (1993) Step dynamics and spiral growth on calcite. Geochimica et Cosmochimica Acta, 57, 491–495.

Gregg, J.M. and Sibley, D.F. (1984) Epigenetic dolomitization and the origin of xenotopic dolomite texture. Journal of Sedimentary Petrology, 54, 908–931.

Gunderson, S.H. and Wenk, H.-R. (1981) Heterogeneous microstructures in oolitic carbonates. American Mineralogist, 66, 789–800.

Hillner, P.E., Manne, S., Gratz, A.J., and Hansma, P.K. (1992) AFM images of dissolution and growth on a calcite crystal. Ultramicroscopy, 42–44, 1387–1393.

Hillner, P.E., Gratz, A.J., Manne, S., and Hansma, P.K. (1992) Atomic-scale imaging of calcite growth and dissolution in real-time. Geology, 20, 359–362.

Khan, M.R. and Barber, D.J. (1990) Composition-related microstructure in zinc-bearing carbonate assemblages from Broken Hill, New South Wales. Mineralogy and Petrology, 41, 229–245.

Lumsden, D.N., Morrison, J.W., and Lloyd, R. (1995) Role of iron and Mg/Ca ratio in dolomite synthesis at 192°C. Journal of Geology, 103, 51–61.

Marquez, X. (1994) Reservoir geology of Upper Devonian Leduc buildups, deep Alberta basin. 285 p. Ph.D. thesis, McGill University, Canada.

Meike, A., Wenk, H.R., O'Keefe, M.A., and Gronsky, R. (1988) Atomic resolution microscopy of carbonates, Interpretation of contrast. Physics and Chemistry of Minerals, 15, 427–437.

Mountjoy, E.W. and Amthor, J.E. (1994) Has burial dolomitization come of age? Some answers from the Western Canada Sedimentary Basin. International Association of Sedimentologists Special Publication, 21. 203–229.

Ortoleva, P.J. (1990) Role of attachment kinetic feedback in the oscillatory zoning of crystals grown from melts. Earth Science Reviews, 29, 3–8.

Paquette, J. and Reeder, R.J. (1990) New type of compositional zoning in calcite: Insights into crystal-growth mechanisms. Geology, 18, 1244–1247.

———(1995) Relationship between surface structure, growth mechanism, and trace element incorporation in calcite. Geochimica et Cosmochimica Acta, 59, 735–749.

Paquette, J., Ward, W.B., and Reeder, R.J. (1993) Chapter 18. Compositional zoning and crystal growth mechanism in carbonates: A new look at microfabrics imaged by cathodoluminescence microscopy. In R. Rezak and D. Lavoie, Eds. Carbonate Microfabrics, p. 243–252. Springer-Verlag, New York.

Paquette, J., Vali, H., and Mucci, A. (1996) TEM study of Pt-C replicas of calcite overgrowths precipitated from electrolyte solutions. Geochimica et Cosmochimica Acta, 60, 4689–4700.

Qing, H. and Mountjoy, E.W. (1994) Petrography and geochemistry of coarse-crystalline and saddle dolomites in the Presqu'ile Barrier: host rocks of MVT deposits and hydrocarbon reservoirs in the Western Canada Sedimentary Basin. American Association of Petroleum Geologists Bulletin 78, 55–77.

Reeder, R.J. (1981) Electron optical investigation of sedimentary dolomites. Contributions to Mineralogy and Petrology, 76, 148–157.

———(1983) Crystal chemistry of the rhombohedral carbonates. In Mineralogical Society of America Reviews in Mineralogy, 11, 1–47.

———(1992a) Growth and alteration microstructure. In Mineralogical Society of America Reviews in Mineralogy, 27, 381–424.

———(1992b) Intrasectoral zoning in dolomite: further evidence for surface structural control on element incorporation during crystal growth. V.M. Goldschmidt Conference Program and Abstracts, A88.

Reeder, R.J. and Prosky, J. (1986) Compositional sector zoning in dolomite. Journal of Sedimentary Petrology, 56, 237–247.

Reeder, R.J., Fagioli, R.O., and Meyers, W.J. (1990) Oscillatory zoning of Mn in solution-grown calcite crystals, 29, 39–46.

Reksten, K. (1990) Modulated microstructure in calcian ankerite, American Mineralogist, 75, 495–500.

Skattula, W. and Horn, L. (1960) Ein einfaches, hochauflösendes Abdruckverfahren für die Elektronenmikroskopie. Experim. Tech. Phys. 8, 1–9 (not seen; extracted from Reviews in Mineralogy, 27, 287, 1992).

Spurr, A.R. (1969) A low-viscosity epoxy resin embedding medium for electron microscopy. Journal of Ultrastructure Research, 26, 31–43.

Staudt, W.J., Reeder, R.J., and Schoonen, M.A.A. (1994) Surface structural controls oon compositional zoning of SO and SeO in synthetic calcite single crystals. Geochimica et Cosmochimica Acta, 58, 2087–2098.

Sunagawa, I. (1987) Surface microtopography of crystal faces. In I. Sunagawa, Ed. Morphology of Crystals. Part A, p. 509–587. Terra Scientific Publishing, Tokyo.

Teng, H.H., Dove, P.M., Orme, C.A., and De Yoreo, J.J. (1998) Thermodynamics of calcite growth: Baseline for understanding biomineral formation. Science 282, 724–727.

Tribble, J.S., Arvidson, R.S., Lane, M., IV, and Mackenzie, F.T. (1995) Crystal chemistry, and thermodynamic and kinetic properties of calcite, dolomite, apatite, and biogenic silica: applications to petrologic problems. Sedimentary Geology, 95, 11–37.

Vaillancourt, J. and Paquette, J. (1995) Zoning patterns of Pb, Mn and Sr in synthetic calcite. Program with Abstracts, 20, p. A-106. GAC/MAC Annual Meeting, Victoria, BC.

Vali, H. and Bachmann, L. (1988) Ultrastructure and flow behaviour of colloidal smectite dispersions. Journal of Colloid and Interface Science, 126(1), 278–291.

Vali, H. and Hesse R. (1990) Alkylammonium ion treatment of clay minerals in ultrathin section: A new method for HRTEM examination of expandable layers. American Mineralogist, 75, 1445–1448.

Vali, H. and Köster, H.M. (1986) Expanding behaviour, structural disorder, regular and random irregular interstratification of 2:1 layer-silicates studied by high-resolution images of transmission electron microscopy. Clay Minerals, 21, 827–859.

Vali, H., Hesse, R., and Kohler, E. (1991) Combined freeze-etch replicas and HRTEM imaging as tools to study the fundamental-particles and the multi-phase nature of 2:1 layer silicates. American Mineralogist, 76, 1973–1984.

Van Tendeloo, G., Gronsky, R.R., and Wenk, H.-R. (1985) Modulated structures in calcian dolomites: A study by electron microscopy. Physics and Chemistry of Minerals, 12, 333–341.

Ward, W.B. and Reeder, R.J. (1993) Chapter 19. The use of growth microfabrics and transmission electron microscopy in understanding replacement processes in carbonates. In R. Rezak and D. Lavoie, Eds., Carbonate Microfabrics, p. 253–264. Springer-Verlag, New York.

Wenk, H.-R. and Zhang, F. (1985) Coherent transformations in calcian dolomites. Geology, 13, 457–460.

Wenk, H.-R., Barber, D.J., and Reeder, R.J. (1983) Microstructure in carbonates. In Mineralogical Society of America Reviews in Mineralogy, 11, 301–367.

MANUSCRIPT RECEIVED AUGUST 20, 1998
MANUSCRIPT ACCEPTED JULY 12, 1999
PAPER HANDLED BY ADRIAN J. BREARLEY